

Stochastic model of randomly end-linked polymer network micro-regions.

Sam C.P. Norris and Andrea M. Kasko

Department of Bioengineering, University of California Los Angeles, Los Angeles, California, USA

Tom Chou

*Department of Computational Medicine and
Department of Mathematics, University of California Los Angeles, Los Angeles, California, USA*

Maria R. D’Orsogna*

Department of Mathematics, California State University Northridge, Northridge, California, USA

(Dated: July 10, 2020)

Polymerization and formation of crosslinked polymer networks are important processes in manufacturing, materials fabrication, and in the case of hydrated polymer networks, synthesis of biomedical materials, drug delivery, and tissue engineering. While considerable research has been devoted to the modeling of polymer networks to determine averaged, mean-field, global properties, there are fewer studies that specifically examine the variance of the composition across “micro-regions” (composed of a large, but finite, number of polymer network strands) within the larger polymer network. Here, we mathematically model the stochastic formation of polymer networks comprised of linear homobifunctional network strands that undergo an end-linking gelation process. We introduce a master equation that describes the evolution of the probabilities of possible network micro-region configurations as a function of time and extent of reaction. We specifically focus on the dynamics of network formation and the statistical variability of the gel micro-regions, particularly at intermediate extents of reaction. We also consider possible annealing effects and study how cooperative binding between the two end-groups on a single network-strand affects network formation. Our results allow for a more detailed and thorough understanding of polymer network dynamics and variability of network properties.

I. INTRODUCTION

The study of crosslinked polymer networks is important in many applications from heavy industry to biomedical research [1–8]. Crosslinked polymer networks can be formed by various techniques, leading to a diverse and complex set of structures and properties. Of these network types, considerable attention has been paid to those formed by a process termed “end-linking”. End-linked networks are usually comprised of polymeric precursors, or “network strands,” that contain N reactive end-groups [9, 10]. During gelation, crosslinks, or “branchpoints,” link multiple end-groups together. For example, poly(ethylene glycol) (PEG)-based hydrogels, which are common in biomedical applications, are typically formed through the reaction of its end-groups [11].

Network strands can bind to form a network via two main polymerization reaction mechanisms: step-growth and chain-growth. Several excellent reviews have been written to describe these processes [11–14]. Briefly, gelation by step-growth polymerization typically involves a defined binary reaction (e.g., thiol-ene or azide-alkyne reactions) between the network strand end-groups and the complementary binding sites of a multifunctional branchpoint which acts to crosslink the network strands together. Networks formed by step-growth polymerization are typically more homogeneous in structure since

the number of functional groups per branchpoint can be fixed. Gelation by chain-growth polymerization occurs via a chain-extension reaction where the network strand end-groups bind to a growing chain of end-groups, termed the “active center” (e.g., free-radical polymerization of vinyl end-groups). The chain of end-groups forms a branchpoint that crosslinks the network strands together. Networks formed by chain-growth polymerization tend to have a more heterogeneous structure since the number of end-groups bound at the branchpoint is not fixed.

Network strands binding via either step- or chain-growth may exist in many states. For bifunctional strands with $N = 2$ reaction sites three possibilities arise as depicted in Figure 1a: (i) the strand may be “free” where neither of the reactive ends have bound (s_0 -strand); (ii) the strand may “dangle” where only a single end has bound and the strand dangles from the rest of the network (s_1 -strand); or (iii) the strand may be “intact” where both ends are bound to the larger polymer network and bridge two different branchpoints (s_2 -strand) [15]. Strands with both ends bound may also form a loop, where both ends are bound to the same branchpoint [16]. The proportion of free, dangling and intact network strands may affect the chemical and physical properties of the network, for example in water-swollen polymeric networks, bound strand ratios impact gel modulus, mesh size, and swelling [3].

Finally, the architecture of polymer networks formed by end-linking gelation is not spatially uniform. Het-

* dorsogna@csun.edu

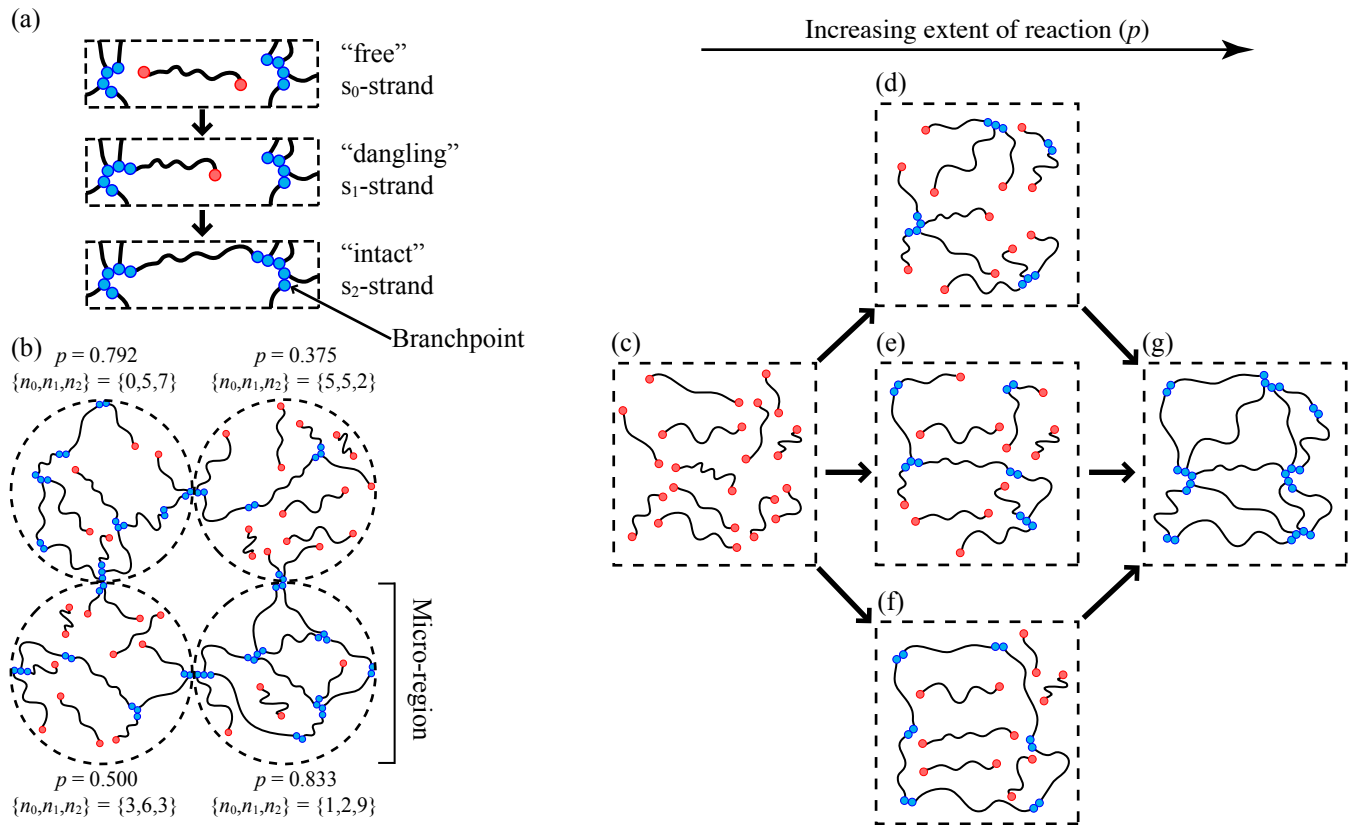


FIG. 1. Polymer network configurations. Black lines represent network strands with $N = 2$ reactive end-groups that can be unbound (red dots) or bound (blue dots). Reactive ends bind to form a branchpoint connecting different strands. (a) Bifunctional strands are either “free” – neither end-group is bound (s_0 -strand); “dangling” – a single end-group is bound (s_1 -strand); or “intact” – both end-groups are bound (s_2 -strand). (b) Schematic of four uncoupled “micro-regions” (dashed lines) within the network. Each is comprised of N_s strands but the extent of reaction p can vary. (c) For $p = 0$ all network strands are in the s_0 -state. (d-f) For intermediate $0 < p < 1$, many configurations are possible, including (d) only s_1 -strands, (e) a combination of s_0 -, s_1 -, and s_2 -strands, or (f) only s_0 - and s_2 -strands. (g) For $p = 1$, the only possible configuration is for strands be fully bound in the s_2 -state.

erogeneous domains within polymer networks exist that span a few to hundreds of nanometers in size and arise through variations in local strand concentration (termed “frozen concentration fluctuation”), heterogeneous distribution of crosslinking, or topological- and connectivity-based inhomogeneities due to variability in network strand assembly [17–20]. We define these microscopic domains as “micro-regions.” For simplicity we assume micro-regions are statistically identical, independent, and composed of a fixed number N_s of strands. Each strand is also assumed to carry $N = 2$ reactive end groups, the most representative experimental scenario [9], resulting in a total of $2N_s$ available binding sites per micro-region. We also denote by m the number of bound end-groups in each micro-region, so that the fraction p of bound end-groups per micro-region is $p = m/(2N_s)$. This quantity is also known as the extent of reaction, and can be experimentally tuned to control the elastic modulus, viscosity, swelling, mesh size, and other network properties[2]. By definition $0 \leq p \leq 1$ since the number of bound end groups m cannot exceed

the total number of available ones $2N_s$. Finally we assume that micro-regions are large enough that boundary effects between bordering domains are negligible so that the free, dangling, intact strand distribution of two adjacent micro-regions are not correlated. Note that the same value of $0 < p < 1$, may be associated to different $\{n_0, n_1, n_2\}$ micro-region configurations with n_0 free, n_1 dangling, and n_2 intact strands. Figure 1b shows four different micro-region realizations within a larger network where N_s is fixed but different $\{n_0, n_1, n_2\}$ configurations arise, resulting in different extents of reaction p . In Figure 1d-f we show several distinct $\{n_0, n_1, n_2\}$ configurations corresponding to fixed N_s and p .

Some quantities of interest may be derived using p such as the likelihood $P_\ell(p)$ [1, 2, 15, 21, 22] of finding free ($\ell = 0$), dangling ($\ell = 1$), and intact ($\ell = 2$) strands for a given p . A stochastic analysis however would lead to an expression for the probability distribution of finding any micro-region configuration $\{n_0, n_1, n_2\}$ corresponding to a given p , offering a much richer understanding of the binding process. Previously developed stochastic

models use a subset-of-states approach[23–25], where a polymerizing mixture is described as a set of “subgraph” states of monomeric strands, a subset of which is used to drive polymerization[26, 27]. These models, however, only examine the connectivity of small subgraphs, typically made of only a few network strands, to represent large scale networks and predict bulk quantities such as the network gel point [26, 28]. Studies involving larger subgraphs containing a sizable number of strands (say, greater than ten) are still lacking. Finally, although several Monte Carlo numerical studies have examined network heterogeneity[29–35], none of them have evaluated configuration probability distributions.

We aim to determine the probability distribution for a given configuration of free, dangling, and intact strands within a micro-region of N_s bifunctional strands, given a total number of m bound end-groups, or equivalently for fixed $p = m/2N_s$. This will allow us to go beyond the characterization of a micro-region by means of p and N_s alone and to obtain analytical expressions for micro-region properties that depend on possible $\{n_0, n_1, n_2\}$ configurations. In some experimental scenarios m or p may change among micro-region realizations, and it may be useful to understand the structure of the network for a given average, intermediate extent of reaction $\langle p \rangle$. Our results will thus be presented both as a function of time, and of the average extent of reaction. We draw on existing stochastic self assembly and nucleation models[36–40] and utilize a master equation approach. Different forms of the master equation will be developed and analyzed to account for different end-group reactivities and the possibility for end-groups to dynamically rearrange within the micro-region. We do not model branchpoint functionality but focus on the number of intact, dangling, and free $\{n_0, n_1, n_2\}$ strands within micro-regions. As a result, the total number of branchpoints and topology of the network do not affect our modeling, so while the structures depicted in Figure 1 resemble those formed by chain-growth polymerization, our methods can be easily applied to step-growth polymerization as well. Table I lists the various quantities used in the remainder of this work.

II. MATHEMATICAL MODELS AND ANALYSIS

For completeness, we first review basic combinatoric and equilibrium models describing network formation before introducing our master equation models.

A. Combinatoric and equilibrium models

Many mathematical studies of network formation via end-linking have used combinatoric approaches to quantify the number of polymeric strands in a given state [15, 41–44]. The extent of reaction p , defined as the fraction of bound end-groups per micro-region, can also be

interpreted as the probability that any end-group within a micro-region has bound. The probability $P_\ell(p)$ of finding an s_ℓ -strand with $0 \leq \ell \leq N$ bound end-groups is thus

$$P_\ell(p) = \binom{N}{\ell} p^\ell (1-p)^{N-\ell}, \quad (1)$$

which assumes that of N end-groups, ℓ are bound and $N - \ell$ are not. Equation 1 provides a basis for mean field end-linking gelation models used to predict network properties. Henceforth we assume $N = 2$. The average number $n_\ell(p)$ of s_ℓ -strands within a micro-region of N_s strands can thus be written as

$$n_\ell(p) = N_s \binom{2}{\ell} p^\ell (1-p)^{2-\ell}. \quad (2)$$

Equation 2 does not provide any information on the possible spatial arrangement of free, dangling, intact, strands within a micro-region. Some end-groups may also bind differently than others depending on their state. For example free strands might more readily bind than dangling ones since diffusion allows them to more easily navigate the local environment to find an appropriate reaction site. Cooperative binding arises when the unbound end-group of a dangling strand more readily binds to form a fully bound, intact strand due to its proximity to the polymerizing network, especially when the polymer solution is dilute. Uncooperative binding emerges when s_2 -strand formation from the binding of an existing s_1 -strand is hindered by negative allosteric effects, which has been shown to occur in rigid strands [35]. Finally, the reaction steps associated with network formation may also be irreversible or reversible. Irreversible reactions lead to “quenched” network formation whose properties are highly dependent on initial conditions, while reversible reactions allow the network to rearrange while forming and “anneal.”

The binding scenarios described above lead to different probability distributions for a given micro-region configuration. Evaluating these distributions requires a more complex mathematical representation than Equations 1 or 2. Some can be derived via combinatoric arguments, for example in the case of reversible binding, when equilibrium is reached and the annealing process is complete. We evaluate such limit here and find the probability distribution for a given micro-region configuration $\{n_0, n_1, n_2\}$ with n_0 unbound s_0 -strands, n_1 singly bound s_1 -strands, and n_2 doubly bound s_2 -strands, under the assumption that a total of m end-groups have bound.

At equilibrium, the time and order at which strands were linked do not affect configuration likelihoods, so the task of finding the probability distribution for $\{n_0, n_1, n_2\}$ is equivalent to finding the number of ways $\mathcal{N}(n_0, n_1, n_2)$ one can distribute $\{n_0, n_1, n_2\}$ among N_s strands with m total bindings. The above quantities are related by $n_0 + n_1 + n_2 = N_s$ since all strands must be accounted for, and by $n_1 + 2n_2 = m$ to include the contribution of each strand type to the total bound end-group

TABLE I. Summary of variables used.

Symbol	Representation
N	Number of reactive end-groups per network strand
ℓ	Number of bound end-groups per network strand
s_ℓ	Designation of strand type with ℓ bound end-groups
N_s	Number network strands per micro-region
n_0	Number of s_0 -network strands per micro-region
n_1	Number of s_1 -network strands per micro-region
n_2	Number of s_2 -network strands per micro-region
m	Total number of bound end-groups per micro-region
p	Extent of reaction, $m/(N_s N)$
t	Time of reaction (time units)
$P(n_1, n_2, t)$	Micro-region configuration $\{n_0, n_1, n_2\}$ probability at t
α	Reactivity/cooperative binding parameter (unitless)
λ	Binding rate (time^{-1})
κ	End-group rearrangement rate to binding rate ratio (unitless)

count. Hence, a given micro-region with configuration $\{n_0, n_1, n_2\}$ can be equivalently described by $\{N_s, m, n_2\}$. The extent of reaction p can also be determined from $\{N_s, m, n_2\}$ via $p = m/(2N_s)$. Combinatoric arguments yield $\mathcal{N}(n_0, n_1, n_2)$ as

$$\mathcal{N}(n_0, n_1, n_2) = 2^{n_1} \binom{N_s}{n_0 \ n_1 \ n_2}. \quad (3)$$

Here, the 2^{n_1} factor arises from the fact that the bound end-group on an s_1 -strand can be arranged in two configurations per strand. The above can be rewritten using $n_0 = N_s - m + n_2$ and $n_1 = m - 2n_2$ as follows

$$\mathcal{N}(N_s, m, n_2) = \frac{2^{m-2n_2} N_s!}{(N_s - m + n_2)! (m - 2n_2)! n_2!}. \quad (4)$$

Upon summing over n_2 with N_s, m fixed, we find $Z_{N_s, m}$ the partition function over all possible configurations, with N_s, m fixed

$$Z_{N_s, m} = \sum_{n_2=0}^{[m/2]} \mathcal{N}(N_s, m, n_2), \quad (5)$$

where $[\cdot]$ indicates the integer part of its argument. The equilibrium probability distribution can finally be calculated as

$$P_{N_s, m}(n_2) = \frac{\mathcal{N}(N_s, m, n_2)}{Z_{N_s, m}}. \quad (6)$$

Equation 6 may be used to evaluate many different micro-region properties, such as averages, variances, and higher moments. We begin with the average number of free, dangling, and intact strands, respectively given by

$$\langle n_0 \rangle = N_s - m + \sum_{n_2=0}^{[m/2]} n_2 P_{N_s, m}(n_2). \quad (7a)$$

$$\langle n_1 \rangle = m - 2 \sum_{n_2=0}^{[m/2]} n_2 P_{N_s, m}(n_2), \quad (7b)$$

$$\langle n_2 \rangle = \sum_{n_2=0}^{[m/2]} n_2 P_{N_s, m}(n_2). \quad (7c)$$

In Equations 7 the average, denoted by $\langle \cdot \rangle$, is taken across all micro-regions with the same N_s and m , or equivalently, using all possible configurations within a single micro-region with N_s strands and m total number of bound end-groups. The above combinatoric argument assumes that end-group binding is accompanied by end-group annealing until equilibrium is reached, independent of the number of bound end-groups already present. However, within cooperative or uncooperative binding, bound end-groups may promote or hinder the binding of other end-groups. We include these phenomena by rewriting Equation 4 as

$$\mathcal{N}(N_s, m, n_2, \alpha) = \frac{(2/\alpha)^{m-2n_2} N_s!}{(N_s - m + n_2)! (m - 2n_2)! n_2!}, \quad (8)$$

where the reactivity parameter $\alpha > 1$ represents cooperative binding, penalizing dangling ends in favor of $s_1 \rightarrow s_2$ events. Values of $\alpha < 1$ represent uncooperative binding where $s_0 \rightarrow s_1$ events are favored. The neutral case is $\alpha = 1$. Finally, the equilibrium probability distribution $P_{N_s, m, \alpha}(n_2)$ can be written as

$$P_{N_s, m, \alpha}(n_2) = \frac{\mathcal{N}(N_s, m, n_2, \alpha)}{\sum_{n_2=0}^{[m/2]} \mathcal{N}(N_s, m, n_2, \alpha)}. \quad (9)$$

We plot $P_{N_s, m, \alpha}(n_2)$ in Equation 9 for several values of n_2 , under three choices of α and as a function of the

extent of reaction $p = m/(2N_s)$ in Figures 2a–c. The solid lines connect micro-region configurations with the same n_2 ; we choose this representation as the number of intact “elastically effective” s_2 -network strands is an important feature of polymer networks and determines both the mechanical modulus and swelling behavior of the network [3]. As α increases, all curves tend to shift to the left, as might be expected since increasing cooperative effects favor the emergence of s_2 -strands for a given p . In Figure 2d we plot the average strand fractions $\langle n_\ell \rangle / N_s$ for $\ell = 0, 1, 2$ as evaluated via Equations 7 for $N_s = 40$ and as a function of p . Note that for any α , the average quantity $\langle n_1 \rangle$ is a symmetric function of m about N_s as can be verified by imposing $m' = 2N_s - m$ in Equation 7b and verifying that $\langle n_1 \rangle$ remains unchanged. Since $p = m/2N_s$, this also implies that $\langle n_1 \rangle$ will be symmetric about $p = 1/2$ for all values of α , as seen in Figures 2e–f. We also calculate the second moment $\langle n_2^2 \rangle$ defined as

$$\langle n_2^2 \rangle = \sum_{n_2=0}^{\lfloor m/2 \rfloor} n_2^2 P_{N_s, m, \alpha}(n_2), \quad (10)$$

from which we obtain the variance $\text{Var}(n_2) = \langle n_2^2 \rangle - \langle n_2 \rangle^2$ where $\langle n_2 \rangle$ is derived in Equation 7c. Similarly as for $\langle n_1 \rangle$ one can verify that $\text{Var}(n_2)$ is symmetric about $p = 1/2$ for all values of α . Since $n_1 = m - 2n_2$, $n_0 = N_s - m + n_2$, and given $\langle n_1 \rangle$ and $\langle n_0 \rangle$ from Equations 7a–b, $\text{Var}(n_1) = \langle n_1^2 \rangle - \langle n_1 \rangle^2$ and $\text{Var}(n_0) = \langle n_0^2 \rangle - \langle n_0 \rangle^2$ can also be derived using Equations 7c and 10. Figure 2e shows $\text{Var}(n_2)/N_s^2$ as a function of p for different values of α . In each case, the maximum variance occurs when half of all possible end-groups have bound at $p = 1/2$. As α deviates from the neutral condition $\alpha = 1$, the bias towards certain bond types induced by cooperativity or uncooperativity causes the variance to decrease. In Figure 2f we plot $\text{Var}(n_2)/N_s^2$ as a function of p for different values of N_s : the curve remains symmetric about $p = 0.5$ and as N_s increases, the normalized variance decreases.

B. Dynamic models: Master Equation approaches

We now derive the probability distribution $P(n_0, n_1, n_2, t)$ of finding a given $\{n_0, n_1, n_2, t\}$ micro-region configuration at time t through a master equation that allows for the inclusion of reversible/irreversible (annealed/quenched) bond formation, and cooperative/uncooperative binding. Since the total number of strands per micro-region is constant, the constraint $n_0 + n_1 + n_2 = N_s$ is obeyed at all times and effectively $P(n_0, n_1, n_2, t) \rightarrow P(n_1, n_2, t)$. We compare equilibrium or steady state solutions to Equation 1; where possible we also determine the full time-dependent solution for $P(n_1, n_2, t)$, which can be used to derive other quantities of interest, such as the variance and higher moments.

1. Quenched end-group binding

The first case we consider is that of irreversible (or quenched) end-group binding, whereby once an end-group has bound, it will not detach. We also assume the binding rate λ of an end-group is constant. Under these conditions, the master equation for the probability distribution $P(n_1, n_2, t)$ evolves according to

$$\begin{aligned} \frac{dP(n_1, n_2, t)}{dt} = & 2\lambda(N_s - n_1 - n_2 + 1)P(n_1 - 1, n_2, t) \\ & + \lambda\alpha(n_1 + 1)P(n_1 + 1, n_2 - 1, t) \\ & - \lambda[2(N_s - n_1 - n_2) + \alpha n_1]P(n_1, n_2, t), \end{aligned} \quad (11)$$

where we have explicitly used the $n_0 = N_s - n_1 - n_2$ constraint. Equation 11 also includes the reactivity parameter α : $\alpha > 1$ represents cooperative binding so that $s_1 \rightarrow s_2$ binding events are more likely than $s_0 \rightarrow s_1$ events; the reverse is true for uncooperative binding, $\alpha < 1$, where $s_0 \rightarrow s_1$ events are favored. The first term on the right hand side of Equation 11 represents the process of an unbound strand attaching to the network structure to form a singly bound dangling strand ($s_0 \rightarrow s_1$), which gives the configuration transition $\{n_0 + 1, n_1 - 1, n_2\} \rightarrow \{n_0, n_1, n_2\}$ (Figure 3). The multiplicative factor $N_s - n_1 - n_2 + 1$ represents the number s_0 -strands in the starting configuration that can bind to the network; the two prefactor is included since an s_0 -strand can bind to the network at either of its two unbound end-groups. Similarly, the second term represents an unbound end-group from a singly bound strand binding to the network and forming a doubly bound strand ($s_1 \rightarrow s_2$). The related transition is $\{n_0, n_1 + 1, n_2 - 1\} \rightarrow \{n_0, n_1, n_2\}$ (Figure 3). The multiplicative factor $n_1 + 1$ represents the number of s_1 -strands that can bind to the network to form an s_2 -strand. Finally the last term describes the processes that drives the system out of the $\{n_0, n_1, n_2\}$ configuration, where either an $s_0 \rightarrow s_1$ transition, with $\{n_0, n_1, n_2\} \rightarrow \{n_0 - 1, n_1 + 1, n_2\}$, or an $s_1 \rightarrow s_2$ transition, with $\{n_0, n_1, n_2\} \rightarrow \{n_0, n_1 - 1, n_2 + 1\}$ occur (Figure 3). The total number of distinct $\{n_0, n_1, n_2\}$ states can be enumerated via

$$\sum_{n_2=0}^{N_s} \sum_{n_1=0}^{N_s - n_2} 1 = \frac{(N_s + 2)(N_s + 1)}{2}. \quad (12)$$

Due to the irreversibility of the binding process, at $t \rightarrow \infty$ we expect the system to consist only of s_2 -network strands: $P(n_1, n_2, t \rightarrow \infty) = 0$ for all $\{n_1, n_2\} \neq \{0, N_s\}$ and $P(0, N_s, t \rightarrow \infty) = 1$ as depicted in Figure 1g. We can obtain an alternate representation for Equation 11 by using the $n_0 + n_1 + n_2 = N_s$ constraint to represent n_2 so that $P(n_0, n_1, n_2, t) \rightarrow P(n_0, n_1, t)$ and the master

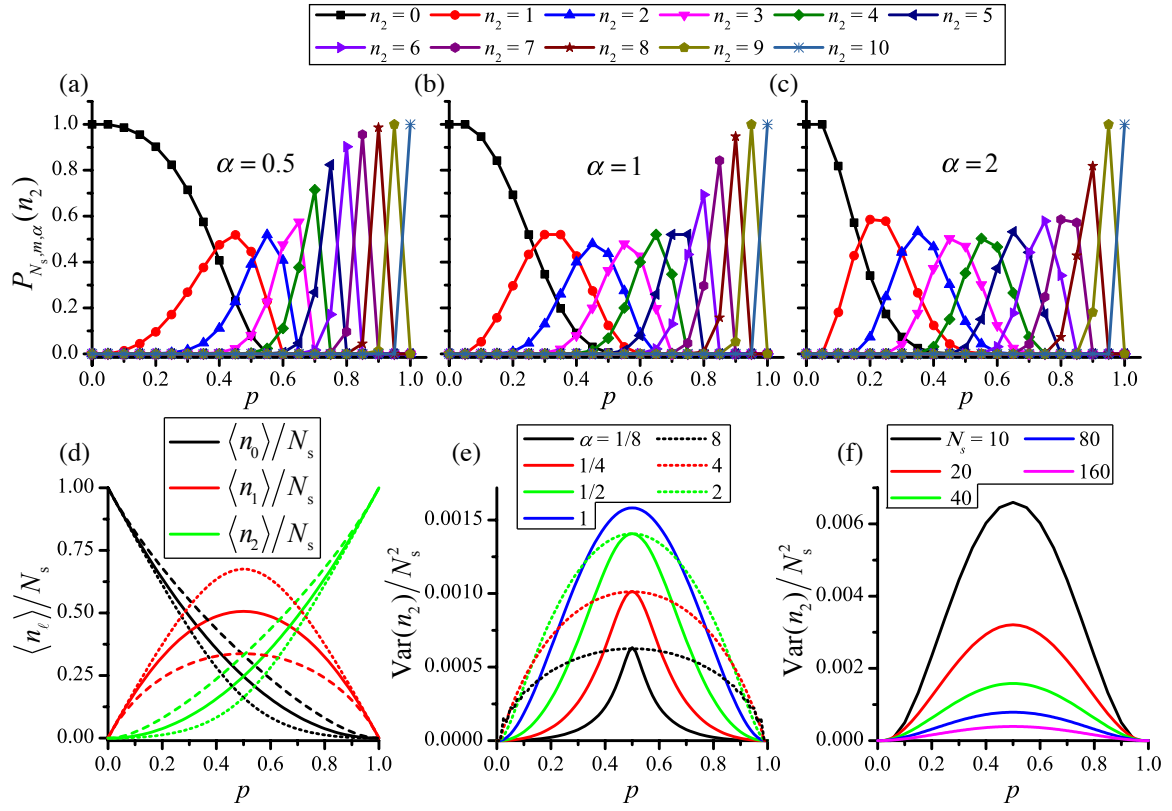


FIG. 2. Results from the equilibrated distribution $P_{N_s, m, \alpha}(n_2)$ as evaluated from Equation 9 for $N_s = 10$ and as a function of the extent of reaction $p = m/2N_s$ for (a) $\alpha = 0.5$, (b) $\alpha = 1$, and (c) $\alpha = 2$. Each point represents a different configuration $\{n_0, n_1, n_2\}$; those with the same n_2 are connected by lines. (d) Average populations $\langle n_\ell \rangle / N_s$ for $\ell = 0, 1, 2$, $N_s = 40$ and $\alpha = 0.5$ (dotted line), $\alpha = 1$ (solid line) and $\alpha = 2$ (dashed line). (e) The normalized variance of n_2/N_s as a function of p for $N_s = 40$, and several values of α . (f) The normalized variance of n_2/N_s for $\alpha = 1$, and several values of N_s . A maximum emerges at $p = 0.5$, whose value decreases with N_s . Notice the symmetry in $\langle n_1 \rangle$ and $\text{Var}(n_2)/N_s^2$ about $p = 0.5$ for all values of α .

equation reads

$$\begin{aligned} \frac{dP(n_0, n_1, t)}{dt} = & 2\lambda(n_0 + 1)P(n_0 + 1, n_1 - 1, t) \\ & + \lambda\alpha(n_1 + 1)P(n_0, n_1 + 1, t) \\ & - \lambda(2n_0 + \alpha n_1)P(n_0, n_1, t). \end{aligned} \quad (13)$$

This representation is equivalent to Equation 11 and will be useful in deriving the distribution $P(n_0, n_1, t)$ from which $P(n_1, n_2, t)$ can be obtained. We now nondimensionalize our model by measuring time in units of the typical bond formation time, λ^{-1} . Henceforth, time t will be dimensionless and λ will no longer appear (equivalently, we set $\lambda = 1$ in Equations 11 and 13). The mean number of strand types $\langle n_\ell(t) \rangle$ in a single micro-regions are defined by

$$\langle n_\ell(t) \rangle = \sum_{n_1, n_2} n_\ell P(n_1, n_2, t), \quad (14)$$

for $\ell = 1, 2$, under the $0 \leq n_1 + n_2 \leq N_s$ constraint. The corresponding mass-action equations can be derived by multiplying Equation 11 by n_ℓ and by summing over

n_1, n_2 under the same constraint so that

$$\frac{d\langle n_0(t) \rangle}{dt} = -2\langle n_0 \rangle, \quad (15a)$$

$$\frac{d\langle n_1(t) \rangle}{dt} = 2\langle n_0 \rangle - \alpha\langle n_1 \rangle, \quad (15b)$$

$$\frac{d\langle n_2(t) \rangle}{dt} = \alpha\langle n_1 \rangle. \quad (15c)$$

Equations 15a-c can be solved under the initial condition $n_0(0) = N_s$, representing all strands being unbound at $t = 0$. We find

$$\langle n_0(t) \rangle = N_s e^{-2t}, \quad (16a)$$

$$\langle n_1(t) \rangle = N_s \frac{2(e^{-\alpha t} - e^{-2t})}{2 - \alpha}, \quad (16b)$$

$$\langle n_2(t) \rangle = N_s \left(1 + \frac{\alpha e^{-2t} - 2e^{-\alpha t}}{2 - \alpha} \right), \quad (16c)$$

so that $\langle n_\ell(t \rightarrow \infty) \rangle \rightarrow 0$ for $\ell = 0, 1$ and $\langle n_2(t \rightarrow \infty) \rangle \rightarrow N_s$. Equations 16a-c represent average values calculated across all micro-regions at time t under quenched binding. We compare the $t \rightarrow \infty$ limit of Equations 16a-c

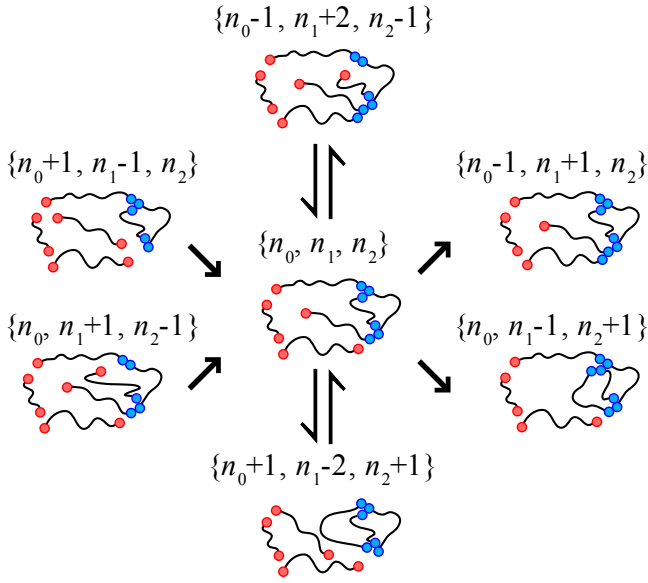


FIG. 3. Possible end-group binding transitions for $N_s = 6$. The state at the center of the schematic is $\{n_0, n_1, n_2\} = \{2, 2, 2\}$ corresponding to $m = 6$. To the left are two $m = 5$ and to the right are two $m = 7$ configurations. Under quenched binding discussed in Section II B 1 the dynamics will flow from left to right following the unidirectional arrows. To the top and bottom of the $\{n_0, n_1, n_2\} = \{2, 2, 2\}$ state are other $m = 6$ configurations. Under dynamic rearrangement discussed in Section II B 2 the system equilibrates following the vertical lines.

to Equation 2 which estimates average strand numbers using combinatoric arguments. To do so, we evaluate $\langle m \rangle = \langle n_1 \rangle + 2\langle n_2 \rangle$ to find

$$\langle m(t) \rangle = \frac{2N_s}{2-\alpha} (2 - \alpha - e^{-\alpha t} + (\alpha - 1)e^{-2t}). \quad (17)$$

from which we calculate the average extent of reaction $\langle p(t) \rangle = \langle m(t) \rangle / 2N_s$

$$\langle p(t) \rangle = 1 - \frac{1}{2-\alpha} [e^{-\alpha t} - (\alpha - 1)e^{-2t}], \quad (18)$$

Inverting the transcendental Equations 17 and 18 for general α is not possible, however, under neutral cooperativity $\alpha = 1$, we find

$$\langle p(t) \rangle = 1 - e^{-t}. \quad (19)$$

A simple analysis of Equations 18 and 19 reveals that $\langle p(t) \rangle$ is a monotonically increasing function of t for all $\alpha > 0$, which is expected given that end-groups bind but do not unbind. For $\alpha = 1$, Equations 16 can be recast as

$$\langle n_0 \rangle = N_s(1 - \langle p \rangle), \quad (20a)$$

$$\langle n_1 \rangle = 2N_s \langle p \rangle (1 - \langle p \rangle), \quad (20b)$$

$$\langle n_2 \rangle = N_s \langle p \rangle^2. \quad (20c)$$

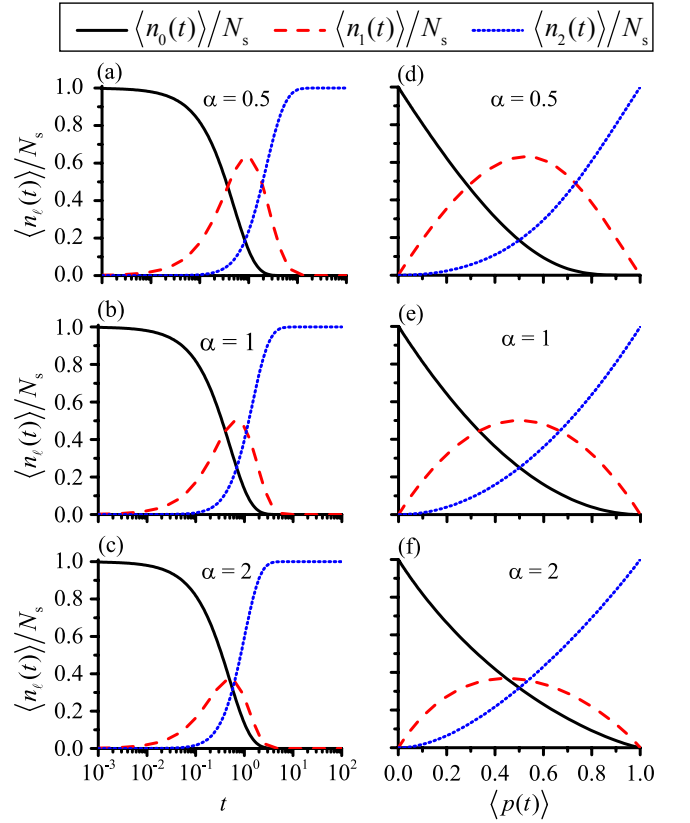


FIG. 4. Average strand fractions $\langle n_\ell(t) \rangle / N_s$ for $\ell = 0, 1, 2$ and $N_s = 40$ as evaluated from Equations 16 and plotted as a function of (a-c) time and (d-f) parametrically against the extent of reaction $\langle p(t) \rangle$ given by Equation 18. The chosen values of the reactivity parameter α are: (a,d) $\alpha = 0.5$, (b,e) $\alpha = 1$, and (c,f) $\alpha = 2$.

Equations 20 have the same form as Equation 2, obtained using mean-field arguments. This implies that the mean-field approach for a given extent of reaction p and $\alpha = 1$ corresponds to an irreversible (quenched) stochastic process halted at time t^* such that $\langle p(t^*) \rangle$ in Equation 19 satisfies $\langle p(t^*) \rangle = 1 - e^{-t^*} = p$. We plot the normalized average strand numbers $\langle n_\ell(t) \rangle / N_s$ as a function of time and as derived from Equations 16a-c in Figure 4a-c, for $N_s = 40$ and different values of α . We find that s_1 -strand formation is favored at smaller α , and s_2 -strand formation is favored at higher α , as might be expected. Since $\langle p(t) \rangle$ is a monotonic function of time we can plot $\langle n_\ell(t) \rangle / N_s$ using Equations 16a-c as parametric equations against $\langle p(t) \rangle$ given in Equation 18. Results are shown in Figure 4d-f for various values of α . These curves differ from those in Figure 2d obtained under equilibration and calculated via Equations 7a-c. Most noticeably, $\langle n_1(t) \rangle$ loses its symmetry about $\langle p(t) \rangle = 0.5$ and becomes skewed.

The master Equation 11 also allows us to derive the time-dependent likelihood of each of the many possible configurations (enumerated in Equation 12), a much more powerful tool than average quantities. For example,

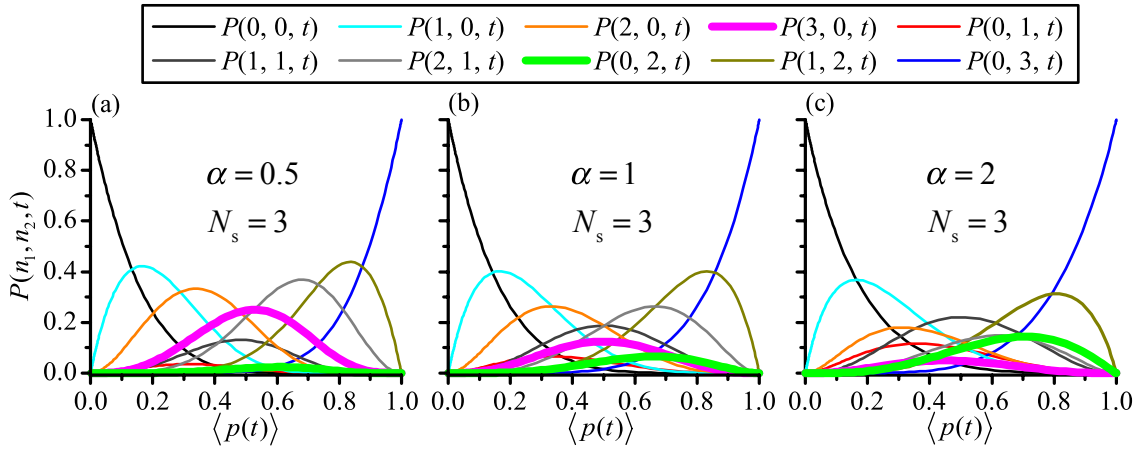


FIG. 5. Probability distributions $P(n_1, n_2, t)$ for $N_s = 3$ under quenched binding as evaluated from Equation 25. We plot $P(n_1, n_2, t)$ parametrically against $\langle p(t) \rangle$ as evaluated from Equation 18 for (a) $\alpha = 0.5$, (b) $\alpha = 1$, (c) $\alpha = 2$. Of the ten possible configurations, two are highlighted: $\{n_0, n_1, n_2\} = \{0, 3, 0\}$ (magenta) and $\{1, 0, 2\}$ (green).

Equation 11 can be solved to find $P(n_1, n_2, t)$ for all times t once the initial condition is specified. We set this to be $P(n_1 = 0, n_2 = 0, t = 0) = 1$, and $P(n_1, n_2, t = 0) = 0$ for all other values of $n_1, n_2 \neq 0$, so that the micro-region is initially made only of free strands. If one chooses to solve Equation 13 to find $P(n_0, n_1, t)$ the equivalent initial conditions are $P(n_0 = N_s, n_1 = 0, t = 0) = 1$ and $P(n_0, n_1, t = 0) = 0$ for $n_0 \neq N_s$ and $n_1 \neq 0$. We solve Equation 13 for $P(n_0, n_1, t)$ rather than Equation 11 for $P(n_1, n_2, t)$ as the analytical computations are simpler. From $P(n_0, n_1, t)$ we can then derive $P(n_1, n_2, t)$ by changing variables through the $n_0 + n_1 + n_2 = N_s$ constraint. To proceed, we introduce the generating function $G(z_0, z_1, t)$ defined as

$$G(z_0, z_1, t) = \sum_{n_0, n_1} P(n_0, n_1, t) z_0^{n_0} z_1^{n_1}, \quad (21)$$

under the constraint $0 \leq n_0 + n_1 \leq N_s$. Upon multiplying Equation 13 by $z_0^{n_0} z_1^{n_1}$ and summing over n_0, n_1 , under the same constraint, we find the following differential equation for $G(z_0, z_1, t)$

$$\frac{\partial G}{\partial t} = 2(z_1 - z_0) \frac{\partial G}{\partial z_0} + \alpha(1 - z_1) \frac{\partial G}{\partial z_1}. \quad (22)$$

Equation 22 is coupled to the corresponding initial condition $G(z_0, z_1, t = 0) = z_0^{N_s}$. Using the method of characteristics, we find

$$G(z_0, z_1, t) = \left[z_0 e^{-2t} + \frac{2z_1 (e^{-\alpha t} - e^{-2t})}{2 - \alpha} + 1 + \frac{\alpha e^{-2t} - 2e^{-\alpha t}}{2 - \alpha} \right]^{N_s}. \quad (23)$$

After performing a Taylor series expansion in z_0, z_1 and

upon comparison with Equation 21 we find

$$P(n_0, n_1, t) = \binom{N_s}{n_0, n_1} e^{-2tn_0} \left(\frac{2(e^{-\alpha t} - e^{-2t})}{2 - \alpha} \right)^{n_1} \times \left(1 + \frac{\alpha e^{-2t} - 2e^{-\alpha t}}{2 - \alpha} \right)^{N_s - n_0 - n_1}. \quad (24)$$

From the constraint $n_0 = N_s - n_1 - n_2$ we can finally write

$$P(n_1, n_2, t) = \binom{N_s}{n_1, n_2} e^{-2t(N_s - n_1 - n_2)} \times \left(\frac{2(e^{-\alpha t} - e^{-2t})}{2 - \alpha} \right)^{n_1} \times \left(1 + \frac{\alpha e^{-2t} - 2e^{-\alpha t}}{2 - \alpha} \right)^{n_2}. \quad (25)$$

Note that $P(n_1, n_2, t \rightarrow \infty) = 0$ for $\{n_1, n_2\} \neq \{0, N_s\}$ and that $P(0, N_s, t \rightarrow \infty) = 1$ as expected from a forward process. Figure 5 shows the probability of individual configurations $P(n_1, n_2, t)$ of micro-regions with $N_s = 3$ plotted parametrically against $\langle p(t) \rangle$ for different values of α . Two different configurations are highlighted: $\{n_0, n_1, n_2\} = \{0, 3, 0\}$ and $\{1, 0, 2\}$. For $\alpha = 2$, when end-group binding is cooperative, the probability of configurations with more s_1 -strands decreases and those with more s_2 -strands increases compared to the neutral ($\alpha = 1$) or uncooperative ($\alpha = 0.5$) cases shown here. In highly cooperative scenarios, once a network strand has bound the transition towards a fully-bound s_2 -strand is fast. In Figure 6a-d we plot the micro-region configuration probabilities $P(n_1, n_2, t)$ as a function of the average extent of reaction $\langle p(t) \rangle$ with increasing N_s . The highest value of $N_s = 40$ we used results in 861 distinct $\{n_0, n_1, n_2\}$ micro-region configurations, as per Equation 12, all with non-zero probability at finite time. Larger values of N_s are possible, but graphically difficult to display.

By inserting the explicit expression for $P(n_1, n_2, t)$ from Equation 25 into Equation 14 we evaluate the average values $\langle n_\ell(t) \rangle$ for $\ell = 1, 2$ to reobtain the same expressions for $\langle n_\ell(t) \rangle$, for $\ell = 0, 1, 2$ already displayed in Equations 16. From Equation 25 we can also calculate the second moments $\langle n_\ell^2(t) \rangle$ as

$$\langle n_\ell^2(t) \rangle = \sum_{n_1, n_2} n_\ell^2 P(n_1, n_2, t) \quad (26)$$

for $\ell = 1, 2$, and the correlation function

$$\langle n_1(t)n_2(t) \rangle = \sum_{n_1, n_2} n_1 n_2 P(n_1, n_2, t) \quad (27)$$

from which we can derive $\langle m^2(t) \rangle$

$$\begin{aligned} \langle m^2(t) \rangle &= \sum_{n_1, n_2} (n_1 + 2n_2)^2 P(n_1, n_2, t) \\ &= \langle n_1^2(t) \rangle + 4\langle n_2^2(t) \rangle + 4\langle n_1(t)n_2(t) \rangle. \end{aligned} \quad (28)$$

Using Equations 16, 17, 26, 27 we find the variances

$$\begin{aligned} \text{Var}(n_\ell(t)) &= \langle n_\ell^2(t) \rangle - \langle n_\ell(t) \rangle^2, \\ \text{Var}(m(t)) &= \langle m^2(t) \rangle - \langle m(t) \rangle^2, \end{aligned} \quad (29)$$

for $\ell = 1, 2$. Finally, $\langle n_0^2(t) \rangle$ is obtained as

$$\begin{aligned} \langle n_0^2(t) \rangle &= \sum_{n_1, n_2} (N_s - n_1 - n_2)^2 P(n_1, n_2, t) \\ &= N_s^2 + \langle n_1^2(t) \rangle + \langle n_2^2(t) \rangle + N_s \langle n_1(t) \rangle \\ &\quad + N_s \langle n_2(t) \rangle + \langle n_1(t)n_2(t) \rangle. \end{aligned} \quad (30)$$

Equations 30 and 16 yield $\text{Var}(n_0(t)) = \langle n_0^2(t) \rangle - \langle n_0(t) \rangle^2$. Explicit expressions for $\langle n_\ell^2(t) \rangle$, $\langle m^2(t) \rangle$, $\text{Var}(n_\ell(t))$ and $\text{Var}(m(t))$ are presented in Section A of the Appendix. In Figure 6e-h we show the parametric plots of the average strand fractions $\langle n_\ell(t) \rangle / N_s$ for $\ell = 0, 1, 2$ against the average extent of reaction $\langle p(t) \rangle$ for several values of N_s . The associated standard deviations calculated as the square root of the variance in Equation 29 are also displayed. As can be expected, fluctuations decrease as N_s increases. Figure 7a shows the parametric plot of $\text{Var}(n_2(t))$ against $\langle p(t) \rangle$ for different values of α and $N_s = 40$. For strong uncooperative binding ($\alpha \rightarrow 0$) and small extents of reaction $\langle p(t) \rangle$, only free strands bind to the network and the variance is very small. However, once all strands have bound at least at one end, and $\langle p(t) \rangle \sim 0.5$, the dangling strands transition to the fully bound state and the variance starts increasing. In Equation A5 of Section A of the Appendix we give an exact analytical expression for $\text{Var}(n_2(t))$; a simple calculation shows that the maximum variance is $N_s/4$ for all values of α , and is attained at smaller average extents of reaction $\langle p(t) \rangle$ as α increases. In Figure 7b we plot the parametric dependence of $\text{Var}(p(t))$ against the average extent of reaction $\langle p(t) \rangle$ with variable α and $N_s = 40$. For very small values of $\alpha \rightarrow 0$, $\text{Var}(p(t))$ is

bimodal and approximately zero at $\langle p(t) \rangle \rightarrow 0.5$. This is because, as discussed above, for $\alpha \rightarrow 0$ end-group binding occurs only on free strands for $\langle p(t) \rangle < 0.5$ and the most likely configurations are those with s_0 and s_1 strands. As $\langle p(t) \rangle \rightarrow 0.5$, only s_1 dangling strands remain so that $\langle n_1(t) \rangle \rightarrow N_s$, $\langle n_1^2(t) \rangle \rightarrow N_s^2$, $\text{Var}(n_2(t)) \rightarrow 0$ and as a result, $\text{Var}(p(t)) \rightarrow 0$. Fully bound strands start emerging for $\langle p(t) \rangle > 0.5$, increasing $\text{Var}(p(t))$. As α increases the variance increases for all $\langle p(t) \rangle$ and the minimum at $\langle p(t) \rangle \sim 0.5$ turns into a maximum. A more detailed discussion is presented in Section B of the Appendix.

In Figure 7c we plot $\text{Var}(n_2(t))/N_s^2$ against $\langle p(t) \rangle$ for different values of N_s ; the curves decrease in magnitude as N_s increases. Finally, in Figure 7d we plot $\langle n_1(t) \rangle / N_s$ parametrically against $\langle p(t) \rangle$ for several values of α . The curves decrease with α once $\langle p(t) \rangle$ is fixed. This also follows from Equation 16b which implies that $\langle n_1(t) \rangle$ is a decreasing function of α for any time t . Since $\langle p(t) \rangle$ is univocally associated to t via Equation 18 it also follows that $\langle n_1(t) \rangle$ is a decreasing function of α for any $\langle p(t) \rangle$. Equations 16b and 18 reveal that the maximum $\langle n_1(t_{\max}) \rangle / N_s = (\alpha/2)^{(1-2/\alpha)}$ is attained at $\langle p(t_{\max}) \rangle = 1 - ((\alpha + 1)/\alpha)e^{-2t_{\max}}$ where $t_{\max} = \ln(2/\alpha)/(2 - \alpha)$. One can easily verify that $\langle p(t_{\max}) \rangle$ is a decreasing function of α as well. These results can be expected as larger α favors the formation of fully bound strands. Thus, for a given average extent of reaction $\langle p(t) \rangle$ the fraction of dangling ends decreases with α , and the maximum is found at an average extent of reaction $\langle p(t) \rangle$ that also decreases with α .

2. Dynamic end-group rearrangement/redistribution

We now consider an equilibration process that allows the bound end-groups in a micro-region to dynamically rearrange, attaching and detaching until thermodynamic equilibrium is reached[45] while maintaining a fixed total number of m bound end-groups. We assume that $m < 2N_s$, ($p < 1$) so that the reaction is not complete and multiple $\{n_0, n_1, n_2\}$ configurations are possible. Experimental realizations include the formation reversible hydrazone bonds [46], imine bonds [47], or guest-host interactions [48]. Here, an intact, s_2 -strand may detach at one of its ends to form a dangling s_1 -strand, while a free s_0 -strand binds to the network to form another s_1 -strand. The reverse process where two s_1 -strands become an s_2 - and s_0 -strand is also possible. In all scenarios $m = n_1 + 2n_2$ is fixed, but there are many distinct ways for the bound end-groups to distribute in s_1 - or s_2 - strands. The final equilibrium configuration is independent of initial conditions so our results will depend only on the selected value of m . We write the reversible

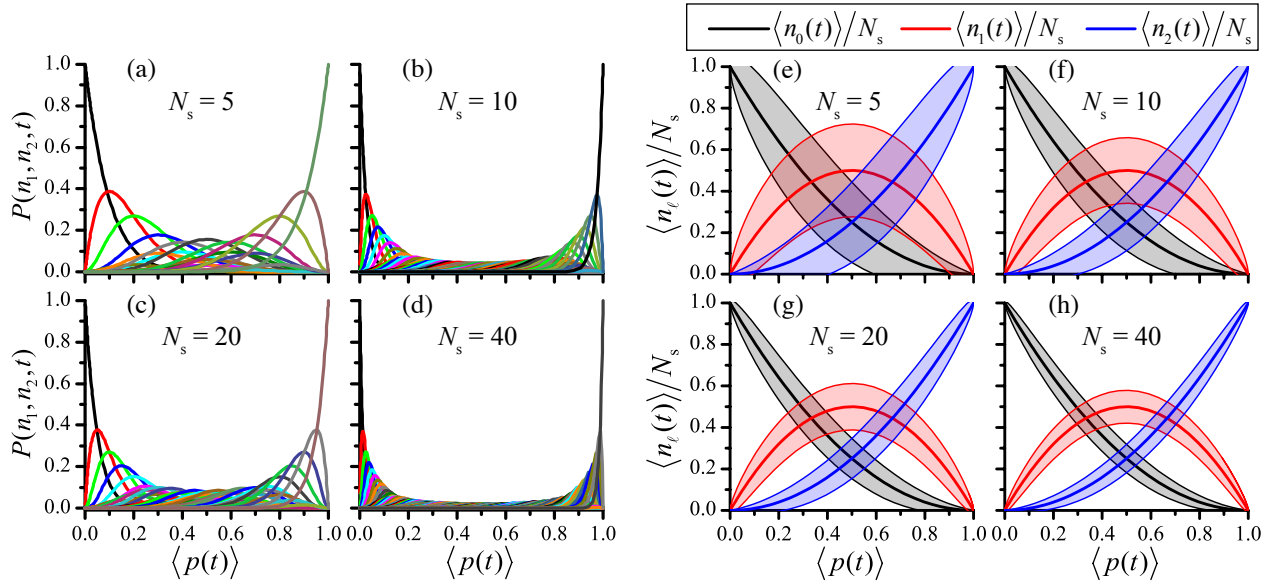


FIG. 6. **(a-d)** Probability distributions $P(n_1, n_2, t)$ for several values of N_s under quenched binding as evaluated from Equation 25. We set $\alpha = 1$ and plot $P(n_1, n_2, t)$ parametrically against $\langle p(t) \rangle$ as evaluated from Equation 18. **(e-h)** Average strand fractions $\langle n_\ell(t) \rangle / N_s$ for $\ell = 0, 1, 2$ plotted parametrically against $\langle p(t) \rangle$. Standard deviations are calculated as the square root of the variance in Equation 29; shaded areas represent the associated error intervals. Chosen N_s values are **(a,e)** $N_s = 5$, **(b,f)** $N_s = 10$, **(c,g)** $N_s = 20$, and **(d,h)** $N_s = 40$.

master equation for $P(n_1, n_2, t)$ as

$$\begin{aligned} \frac{dP(n_1, n_2, t)}{dt} = & 2\kappa\alpha^2 \binom{n_1+2}{2} P(n_1+2, n_2-1, t) \\ & + 4\kappa(N_s - n_1 - n_2 + 1)(n_2 + 1) \\ & \times P(n_1 - 2, n_2 + 1, t) \\ & - 2\kappa\alpha^2 \binom{n_1}{2} P(n_1, n_2, t) \\ & - 4\kappa n_2(N_s - n_1 - n_2)P(n_1, n_2, t). \end{aligned} \quad (31)$$

Here, κ is dimensionless and represents the rearrangement rate measured in terms of the binding rate. The first term on the right hand side of Equation 31 accounts for the formation of a fully bound s_2 -strand and a free s_0 -strand from two dangling s_1 -strands ($2s_1 \rightarrow s_0 + s_2$). Here, the bound end-group of one of the two s_1 -strands exchanges with the unbound end-group of the other leading to the $\{n_0 - 1, n_1 + 2, n_2 - 1\} \rightarrow \{n_0, n_1, n_2\}$ transition. The combinatorial factor enumerates the number of s_1 -strands present in the micro-region and the 2 prefactor represents both s_1 -strands being able to exchange with the other. Finally, the reactivity parameter α is squared, since two dangling ends must bind to form a fully bound strand. The second term represents a fully bound s_2 -strand detaching on one end while promoting the binding of a free s_0 -strand, giving rise to two dangling s_1 -strands. This process is represented by the $\{n_0 + 1, n_1 - 2, n_2 + 1\} \rightarrow \{n_0, n_1, n_2\}$ transition. The factors $(N_s - n_1 - n_2 + 1)$ and $(n_2 + 1)$ represent the number of s_0 - and s_2 -network strands available, respectively. The prefactor 4 accounts for the number of possible bond

movements: either of the two bound end-groups on the s_2 -strand can relocate to either of the two unbound end-groups of the s_0 -strand, yielding a total of four combinations. The last two terms represent the same two processes described above, but driving the system away from $\{n_0, n_1, n_2\}$. Note that there are no terms in Equation 31 representing bonds leaving an s_2 -strand to populate an s_1 -strand; this transition would not change the overall the micro-region configuration $\{n_0, n_1, n_2\}$. The probability $P_b(m, t)$ of having m bound-ends at time t can be written as

$$P_b(m, t) = \sum_{n_2=0}^{\lfloor m/2 \rfloor} P(m - 2n_2, n_2, t), \quad (32)$$

where all possible n_1, n_2 combinations that yield $m = n_1 + 2n_2$ are included. Using Equation 31 it can be easily verified that $P_b(m, t) = P_b(m, t = 0)$. As expected, the master Equation 31 only rearranges the distribution of s_1 and s_2 strands but m remains unchanged. We thus assume the system is initiated with a given m so that $n_1 + 2n_2 = m$ at all times. In addition to this constraint, the number of strands is fixed so that $n_0 + n_1 + n_2 = N_s$. We can thus cast Equation 31 in terms of only one of the n_0, n_1 or n_2 populations. We choose n_2 and determine the steady state $P(n_1, n_2, t \rightarrow \infty) \equiv P^*(n_2)$ by imposing detailed balance between the first and the last term on the right hand side of Equation 31, or equivalently, the second and the third, since it can be easily verified that

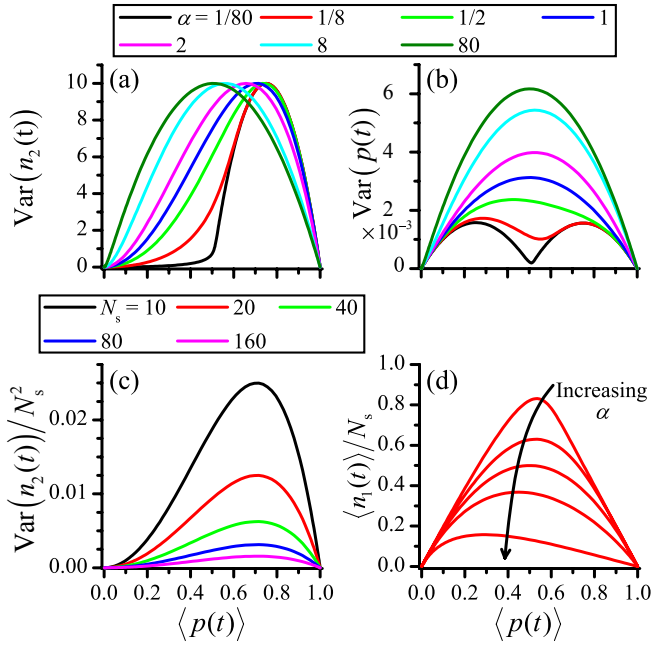


FIG. 7. The variance of the number of (a) s_2 -strands and of (b) bound end-groups m as evaluated by Equations 29 for $\alpha = 1/8, 1/2, 1, 2, \text{ or } 8$ and $N_s = 40$. $\text{Var}(n_2(t))$ and $\text{Var}(p(t))$ are plotted parametrically against $\langle p(t) \rangle$ as evaluated from Equation 18. For $\alpha > 80$ and $\alpha < 1/80$ the curves do not change significantly from those displayed. (c) The variance of the fraction of s_2 -strands $\text{Var}(n_2)/N_s^2$ for $N_s = 10, 20, 40, 80, 160$ and $\alpha = 1$. (d) The relative $\langle n_1(t) \rangle / N_s$ as calculated from Equation 16b for $\alpha = 1/8, 1/2, 1, 2, \text{ or } 8$ and $N_s = 40$.

the conditions are the same. We find

$$\frac{P^*(n_2 - 1)}{P^*(n_2)} = \frac{4n_2(N_s - m + n_2)}{\alpha^2(m - 2n_2 + 2)(m - 2n_2 + 1)}, \quad (33)$$

which can be solved to yield

$$P^*(n_2) = \frac{1}{Z_{m, N_s}} \frac{(2/\alpha)^{m-2n_2} N_s!}{(m - 2n_2)! n_2! (N_s - m + n_2)!}, \quad (34)$$

where Z_{m, N_s} is the normalization constant

$$Z_{m, N_s} = \sum_{n_2=0}^{\lfloor m/2 \rfloor} \frac{(2/\alpha)^{m-2n_2} N_s!}{(m - 2n_2)! n_2! (N_s - m + n_2)!}. \quad (35)$$

This result is the same as Equation 8: the combinatoric approach for a fixed p is equivalent to allowing for relaxation on the network with a fixed number of bound ends and $m = 2pN_s$.

3. End-group rearrangement/redistribution and bond formation

We now consider the two processes of bond formation and redistribution occurring simultaneously and combine

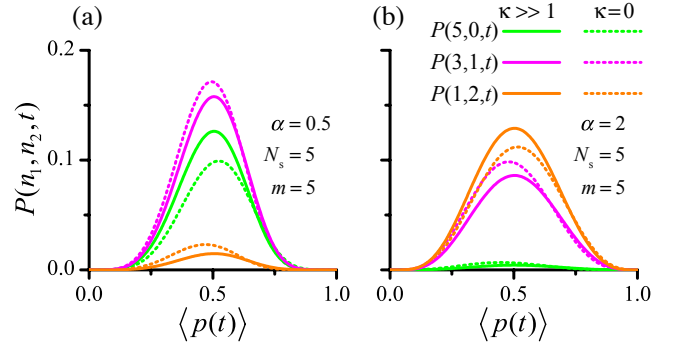


FIG. 8. Configuration probabilities $P(n_1, n_2, t)$ calculated from Equation 36 and plotted parametrically against $\langle p(t) \rangle$ under fast annealing ($\kappa = 1000$, solid lines) and quenched binding ($\kappa = 0$, dashed lines) for $N_s = 5$ and (a) $\alpha = 0.5$, $m = 5$; (b) $\alpha = 2$, $m = 5$.

the two master Equations 11 and 34 so that

$$\begin{aligned} \frac{dP(n_1, n_2, t)}{dt} = & 2(N_s - n_1 - n_2 + 1)P(n_1 - 1, n_2, t) \\ & + \alpha(n_1 + 1)P(n_1 + 1, n_2 - 1, t) \\ & + \kappa\alpha^2(n_1 + 2)(n_1 + 1) \\ & \times P(n_1 + 2, n_2 - 1, t) \\ & + 4\kappa(N_s - n_1 - n_2 + 1)(n_2 + 1) \\ & \times P(n_1 - 2, n_2 + 1, t) \\ & - [\kappa\alpha^2 n_1(n_1 - 1) + 4\kappa n_2(N_s - n_1 - n_2) \\ & + 2(N_s - n_1 - n_2) + \alpha n_1] P(n_1, n_2, t). \end{aligned} \quad (36)$$

Fast annealing, fast binding, and quenched/irreversible binding are modeled by setting $\kappa \gg 1$, $\kappa \ll 1$, and $\kappa = 0$, respectively. Although a full analytical time-dependent solution can not be found, the effects of annealing can be observed in Figure 8. Here we parametrically plot $P(n_1, n_2, t)$ against $\langle p(t) \rangle$ using Equation 36 for $N_s = m = 5$, $\alpha = 0.5$ and $\alpha = 2$, under fast annealing ($\kappa = 1000$) or quenched binding ($\kappa = 0$). Since the rearrangement process allows for more configurations to be explored we expect cooperative effects to be more pronounced under fast annealing, than under quenched binding. In Figure 8a we set $\alpha = 0.5$; since binding is uncooperative, annealing favors configurations with lower values of n_2 . Indeed, the $k = 1000$ curves show an increase in $P(5, 0, t)$ compared to the corresponding $\kappa = 0$ curves, whereas $P(3, 1, t), P(1, 2, t)$ decrease. Similar trends are observed in Figure 8b, where we set $\alpha = 2$. Cooperative binding increases the likelihood of configurations with higher n_2 , so in this case $P(1, 2, t)$ increases while $P(3, 1, t), P(5, 0, t)$ decrease. Note that $P(5, 0, t), P(3, 1, t)$, and $P(1, 2, t)$ all obey the constraint $n_1 + 2n_2 = N_s = 5$. For $\alpha = 2$, and under quenched binding at $\kappa = 0$, Equation 25 yields $P(5, 0, t) = 32e^{-10t}t^5$ which is maximized at $t = 1/2$ corresponding to $\langle p(t = 1/2) \rangle = 1 - 3/2e \neq 1/2$, as per Equ-

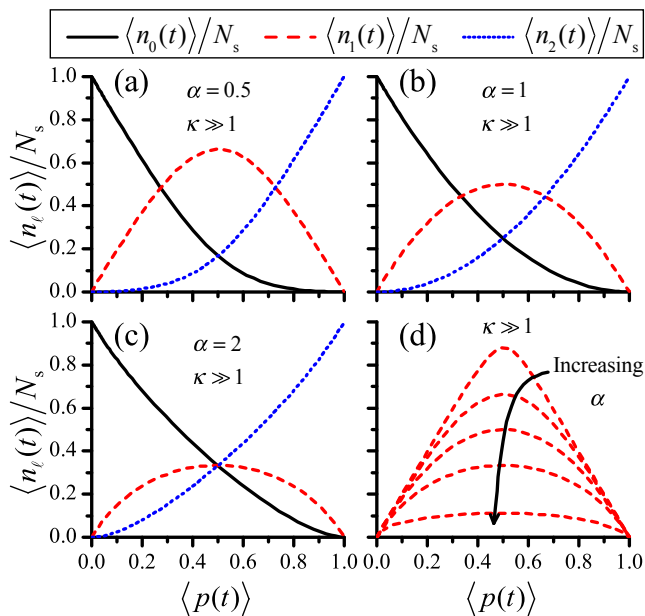


FIG. 9. Average strand fractions $\langle n_\ell(t) \rangle / N_s$ for $\ell = 0, 1, 2$ and $N_s = 10$ evaluated using the probability distribution in Equation 36 and plotted parametrically against $\langle p(t) \rangle$ under fast annealing ($\kappa = 1000$). The reactivity parameter is set as (a) $\alpha = 1$, (b) $\alpha = 0.5$, and (c) $\alpha = 2$. All curves closely resemble those obtained from the equilibrium distribution in Equation 34. (d) Under fast annealing $\langle n_1(t) \rangle / N_s$ is symmetric about $\langle p(t) \rangle = 0.5$ for all α , here set at $\alpha = 1/8, 1/2, 1, 2, 8$, from top to bottom.

tion 18. Similarly, $P(3, 1, t) = 8e^{-8t}t^3(1 - (2t + 1)e^{-2t})$ and $P(1, 2, t) = 2e^{-6t}t(1 - (2t + 1)e^{-2t})$ are also maximized at times that correspond to $\langle p(t) \rangle \neq 1/2$. None of the three distribution curves are thus symmetric about $\langle p(t) \rangle = 1/2$. When $\kappa = 1000$ however the master Equation 36 yields numerical results that are closely aligned with those derived from Equation 31 upon setting $n_1 + 2n_2 = N_s = 5$. This is because annealing is much faster than binding and the time between binding events is much longer than the time for equilibration of a fixed number of bound strands. As a result, once a strand binds, the network can almost fully equilibrate before the next binding event occurs. The curves in Figure 8b for $\kappa = 1000$ thus mirror Equation 34, with the proportions $P(5, 0):P(3, 1):P(1, 2)$ following Equation 33 and become symmetric about $\langle p(t) \rangle = 0.5$ as predicted by Equation 34 when $m = N_s$. The same trends arise when comparing the quenched binding and the fast annealing curves for the uncooperative ($\alpha = 0.5$) case.

In Figure 9 we plot $\langle n_\ell(t) \rangle / N_s$ parametrically against $\langle p(t) \rangle$ for $\alpha = 0.5, 1, 2$ using the probability distribution in Equation 36 for $\ell = 0, 1, 2$ and $\kappa = 1000$. In all cases, the solutions closely match those obtained from the equilibrated distribution in Equation 34 for all values of α as can be seen upon comparison with Figure 2d. The most notable feature is the symmetry of $\langle n_1(t) \rangle$ about $\langle p(t) \rangle = 0.5$ for all α , a feature of the combinatoric ap-

proach, as discussed in Section II A, Intermediate values of $\kappa \approx 1$ yield curves that interpolate between the two extremes $\kappa \gg 1$ and $\kappa = 0$ shown here. Our results imply that networks formed via quenched end-group binding, as per Equation 25, should not be described by models that assume network strands equilibration via redistribution, as per Equations 1 and 9.

III. APPLICATIONS AND CONCLUSIONS

In this work we studied the stochastic properties of bifunctional network strands that undergo an end-linking gelation process. We developed and analyzed a master equation to describe quenched and annealed binding events in micro-regions within a larger polymer network, and include a reactivity parameter to model cooperative effects. While typical models quantify “average” mean-field properties, we are able to evaluate the full probability distribution for any given configuration as a function of time and extent of reaction. By modeling the probability of a configuration within a micro-region, we can propose a crude framework to describe the effects of heterogeneity across the entire sample.

For example, our approach can be used in several polymer network applications under the assumption that a macroscopic region is comprised of a collection of statistically identical, independent, smaller micro-regions. For example, nano/micrometer scale differences in the polymer network properties can affect the fate of cells that are cultured on them [49] as well as the mechanical properties of high-performance materials [50]. If these properties depend on the local number of free, dangling, and intact strands, we can use the relevant probability distribution to evaluate the likelihood of a given configuration $\{n_0, n_1, n_2\}$ in any number of micro-regions sampled by *e.g.*, a cell. The statistical distribution for each micro-region can then be used to construct the probability distribution of the entire macro-system and thus to estimate the chemical or mechanical properties of the polymer network, including their local variability.

Similar considerations can be applied to the study of elastic properties, in particular within phantom network theory which posits that the shear modulus of an ideal network depends on the number density of elastically effective network strands. Our results are readily applicable if we assume that all s_2 -strands in our models are elastically effective and the number of branchpoints is fixed. Starting from the probability $P(n_1, n_2, t)$ that a micro-region is in the $\{n_0, n_1, n_2\}$ configuration, we can also compute the likelihood that a given threshold is met, say, $n_2 \geq n_2^*$. This quantity can then be interpreted as the probability for a “bond” to stretch across a micro-region. One can then calculate the likelihood that a given number of contiguous micro-regions with $n_2 \geq n_2^*$ span the sample through percolation, leading to a dramatic stiffening of the network.

Finally, our work can also be applied to the study of

network degradation, which has attracted much attention over the past two decades as degradable sites have been increasingly incorporated into experimental realizations of end-linking polymerization. These degradable strands typically cleave by enzymatic, hydrolytic, photolytic, or other chemical mechanisms and allow for a reverse gelation process. Here, strands initially exist in the fully bound, intact state where both ends are unreacted. Reverse gelation occurs via reaction or degradation of either end, so that intact strands first become dangling strands, and dangling strands then become free strands. Halting the extent of reaction is common in degradable networks as a way to tune the gel mechanics and this results in a large variability of the micro-region composition. Photodegradable networks [44, 51–55], where end-groups are degraded by exposure to light, are of particular interest as they are uniquely suited to spatially pattern network stiffness, with a high degree of control [56]. Some mathematical models of reverse gelation have been formulated by adapting models of gelation [15]; more specific mean-field photodegradable network models have also been proposed [43, 44]. The present work can be adapted to model degradable networks by associating intact network strands to s_0 -strands (0 degraded end-groups), dangling strands to s_1 -strands (1 degraded end-group), and free strands to s_2 -strands (2 degraded end-groups). Cooperative effects arise in this context as the un-degraded end-groups of an intact strand might more readily react due to tension across the strand induced by network swelling. Once one of the end-groups has cleaved, and the strand dangles, the stress is removed so that the remaining un-degraded end-group is less susceptible to further degradation. Using our stochastic framework, one can calculate the probability of any given micro-region configuration, distinguishing between quenched and annealed network de-gelation reactions. Melting and collapse of rigidity can then be described using percolation concepts.

ACKNOWLEDGMENTS

Funding for this work was provided by the National Institutes of Health through the NIH Director's New Innovator Award Program, 1-DP2-OD008533. S.C.P.N gratefully acknowledges support from a Ruth L. Kirschstein Predoctoral Fellowship (NIH-F31DE026356). T. C. acknowledges support from the NSF through grant DMS-1814364. M.R.D. acknowledges support from the NSF through grant DMS-1814090 and Army Research Office W911NF-16-1-0165. Both T.C. and M.R.D. also acknowledge support from the Army Research Office (W911NF-18-1-0345).

Appendix A: Second moments

We here derive $\langle n_\ell^2(t) \rangle$, $\langle m^2(t) \rangle$, $\text{Var}(n_\ell(t))$ and $\text{Var}(m(t))$ for $\ell = 0, 1, 2$ using the explicit form for

$P(n_1, n_2, t)$ as given in Equation 25. We begin with

$$\langle n_\ell^2(t) \rangle = \sum_{n_2=0}^{N_s} \sum_{n_1=0}^{N_s-n_2} n_\ell^2 P(n_1, n_2, t) \quad (\text{A1})$$

and the associated variances for $\ell = 1, 2$. Using the binomial theorem we find

$$\langle n_1^2(t) \rangle = \frac{2N_s}{(2-\alpha)^2} (e^{-\alpha t} - e^{-2t}) \times [2 - \alpha + 2(N_s - 1)(e^{-\alpha t} - e^{-2t})] \quad (\text{A2})$$

which, coupled with Equation 16b for $\langle n_1(t) \rangle$ leads to

$$\text{Var}(n_1(t)) = \frac{2N_s}{(2-\alpha)^2} (e^{-\alpha t} - e^{-2t}) \times (2 - \alpha - 2e^{-\alpha t} + 2e^{-2t}). \quad (\text{A3})$$

Similarly, Equation A1 for $\ell = 2$ yields

$$\langle n_2^2(t) \rangle = \frac{N_s}{(2-\alpha)^2} (2 - \alpha - 2e^{-\alpha t} + \alpha e^{-2t}) \times [N_s(2 - \alpha - 2e^{-\alpha t} + \alpha e^{-2t}) + 2e^{-\alpha t} - \alpha e^{-2t}], \quad (\text{A4})$$

which coupled with Equation 16c for $\langle n_2(t) \rangle$ leads to

$$\text{Var}(n_2(t)) = \frac{N_s}{(2-\alpha)^2} (2 - \alpha - 2e^{-\alpha t} + \alpha e^{-2t}) \times (2e^{-\alpha t} - \alpha e^{-2t}). \quad (\text{A5})$$

Equation A5 is maximized for time t_M implicitly given by

$$2e^{-\alpha t_M} - \alpha e^{-2t_M} = \frac{2-\alpha}{2} \quad (\text{A6})$$

which corresponds to $\text{Var}(n_2(t_M)) = N_s/4$, independent of the value of α . To evaluate $\langle m^2(t) \rangle$ we must first calculate the correlation function

$$\langle n_1(t)n_2(t) \rangle = \sum_{n_2=0}^{N_s} \sum_{n_1=0}^{N_s-n_2} n_1 n_2 P(n_1, n_2, t) \quad (\text{A7})$$

which yields

$$\langle n_1(t)n_2(t) \rangle = \frac{2N_s(N_s-1)}{(2-\alpha)^2} (e^{-\alpha t} - e^{-2t}) \times (2 - \alpha - 2e^{-\alpha t} + \alpha e^{-2t}) \quad (\text{A8})$$

We can now evaluate $\langle m^2(t) \rangle$ using Equation 28, A2 and A4

$$\langle m^2(t) \rangle = \frac{4N_s^2}{(2-\alpha)^2} [2 - \alpha + (\alpha - 1)e^{-2t} - e^{-\alpha t}]^2 + \frac{2N_s}{(2-\alpha)^2} \left[(2-\alpha)(e^{-\alpha t} + (3-2\alpha)e^{-2t}) - 2((\alpha-1)e^{-2t} - e^{-\alpha t})^2 \right], \quad (\text{A9})$$

from which the variance is obtained as

$$\text{Var}(m(t)) = \frac{2N_s}{(2-\alpha)^2} \left[(2-\alpha) (e^{-\alpha t} + (3-2\alpha)e^{-2t}) - 2 [(\alpha-1)e^{-2t} - e^{-\alpha t}]^2 \right], \quad (\text{A10})$$

where we used Equations 16b-c to evaluate $\langle m(t) \rangle$. Finally, using the constraint $n_0 = N_s - n_1 - n_2$ we find

$$\langle n_0^2(t) \rangle = N_s [N_s e^{-4t} + e^{-2t}(1 - e^{-2t})], \quad (\text{A11})$$

which together with Equation 16a finally yields

$$\text{Var}(n_0(t)) = N_s e^{-2t}(1 - e^{-2t}). \quad (\text{A12})$$

Appendix B: Strong uncooperative binding

All evaluations in the main text assume $\alpha \neq 0$, since the completely uncooperative case ($\alpha = 0$) would not allow for the formation of s_2 strands. Setting $\alpha = 0$ however can be used to explore the short time behavior when $\alpha \rightarrow 0$. This is the case of highly uncooperative binding where although rare, the formation of a fully bound s_2 strand is still possible. Setting $\alpha = 0$ in Equations 16b-c and 18, so that $e^{-\alpha t} \rightarrow 1$ for all times, we find

$$\langle n_1(t) \rangle = N_s(1 - e^{-2t}), \quad (\text{B1})$$

$$\langle n_2(t) \rangle = 0 \quad (\text{B2})$$

$$\langle p(t) \rangle = \frac{1}{2}(1 - e^{-2t}). \quad (\text{B3})$$

Upon setting $\alpha = 0$ in Equation A10 we also find

$$\begin{aligned} \text{Var}(p(t)) &= \frac{1}{4N_s^2} \text{Var}(m(t)) \\ &= \frac{1}{4N_s} e^{-2t}(1 - e^{-2t}) \\ &= \frac{1}{4N_s} 2\langle p(t) \rangle(1 - 2\langle p(t) \rangle). \end{aligned} \quad (\text{B4})$$

Note that Equation B3 yields $\langle p(t) \rangle < 0.5$ for all times, implying that for $\alpha = 0$ the reaction cannot be completed, as expected since fully bound strands cannot emerge. Equation B4 also reveals that $\text{Var}(p(t))$ is symmetric about $\langle p \rangle = 1/4$ and its maximum is attained at $\text{Var}(p(t)) = (16N_s)^{-1}$. The above results still apply in the $\alpha \rightarrow 0$ limit, albeit for $\alpha t \ll 1$ where $e^{-\alpha t} \rightarrow 1$. For example $\text{Var}(p(t))$ follows Equation B4 in Figure 7b up to $\langle p(t) \rangle \sim 0.5$. At longer times, since α is small but not zero, the binding will proceed, and s_2 strands will emerge. We can thus reevaluate Equations 16b-c and 18, for $\alpha \rightarrow 0$ but at long times where $e^{-2t} \rightarrow 0$ and $e^{-\alpha t} \neq 0$ so that

$$\langle n_1(t) \rangle = N_s e^{-\alpha t}, \quad (\text{B5})$$

$$\langle n_2(t) \rangle = N_s(1 - e^{-\alpha t}), \quad (\text{B6})$$

$$\langle p(t) \rangle = 1 - \frac{1}{2}e^{-\alpha t}. \quad (\text{B7})$$

Finally, in the $e^{-2t} \rightarrow 0$ limit, Equation A10 becomes

$$\begin{aligned} \text{Var}(p(t)) &= \frac{1}{4N_s^2} \text{Var}(m(t)) \\ &= \frac{1}{4N_s} e^{-\alpha t}(1 - e^{-\alpha t}) \\ &= \frac{1}{4N_s} 2\langle p(t) \rangle(1 - 2\langle p(t) \rangle). \end{aligned} \quad (\text{B8})$$

The results in Equations B7 and B8 indicate that as $t \rightarrow \infty$, $\langle p(t) \rangle > 0.5$ and $\langle p(t) \rangle \rightarrow 1$. Furthermore, we observe that the shape of $\text{Var}(p(t))$ in Equation B8 is the same as in Equation B4 as also emerges from the bimodal form in Figure 7b. Finally, we note that for $t \rightarrow \infty$, $\langle n_1(t) \rangle \rightarrow 0$, even as $\alpha \rightarrow 0$ since eventually all strands will be fully bound and $\langle n_2(t) \rangle \rightarrow N_s$.

-
- [1] P.-G. De Gennes, *Scaling concepts in polymer physics* (Cornell University Press, 1979).
 [2] P. J. Flory, *Principles of polymer chemistry* (Cornell University Press, 1953).
 [3] M. Rubinstein and R. H. Colby, *Polymer Physics*, June (Oxford University Press, New York, 2003).
 [4] N. A. Peppas, J. Z. Hilt, A. Khademhosseini, and R. Langer, Hydrogels in Biology and Medicine: From Molecular Principles to Bionanotechnology, *Advanced Materials* **18**, 1345 (2006).
 [5] D. Stauffer, A. Coniglio, and M. Adam, Gelation and critical phenomena, in *Polymer Networks*, edited by

- K. Dušek (Springer Berlin Heidelberg, Berlin, Heidelberg, 1982) pp. 103–158.
 [6] N. M. Sangeetha and U. Maitra, Supramolecular gels: Functions and uses, *Chemical Society Reviews* **34**, 821 (2005).
 [7] W. A. Laftah, S. Hashim, and A. N. Ibrahim, Polymer Hydrogels: A Review, *Polymer-Plastics Technology and Engineering* **50**, 1475 (2011).
 [8] P. C. Nicolson and J. Vogt, Soft contact lens polymers: an evolution, *Biomaterials* **22**, 3273 (2001).
 [9] G. Hild, Model networks based on ‘endlinking’ processes: synthesis, structure and properties, *Progress in Polymer*

- Science **23**, 1019 (1998).
- [10] J. E. Mark and J. L. Sullivan, Model networks of endlinked polydimethylsiloxane chains. I. Comparisons between experimental and theoretical values of the elastic modulus and the equilibrium degree of swelling, *The Journal of Chemical Physics* **66**, 1006 (1977).
- [11] C.-C. Lin and K. S. Anseth, PEG Hydrogels for the Controlled Release of Biomolecules in Regenerative Medicine, *Pharmaceutical Research* **26**, 631 (2009).
- [12] J. L. STANFORD, R. F. T. STEPTO, and R. H. STILL, Formation and Properties of Polymer Networks, in *Chemical & Engineering News*, ACS Symposium Series, Vol. 243, edited by S. S. Labana and R. A. Dickie (American Chemical Society, Washington, D.C., 1984) pp. 1–20.
- [13] L. Mespouille, J. L. Hedrick, and P. Dubois, Expanding the role of chemistry to produce new amphiphilic polymer (co)networks, *Soft Matter* **5**, 4878 (2009).
- [14] S. J. Buwalda, K. W. Boere, P. J. Dijkstra, J. Feijen, T. Vermonden, and W. E. Hennink, Hydrogels in a historical perspective: From simple networks to smart materials, *Journal of Controlled Release* **190**, 254 (2014).
- [15] A. T. Metters, C. N. Bowman, and K. S. Anseth, A Statistical Kinetic Model for the Bulk Degradation of PLA- b -PEG- b -PLA Hydrogel Networks, *The Journal of Physical Chemistry B* **104**, 7043 (2000).
- [16] A. E. Tonelli and E. Helfand, Elastically Ineffective Cross-Links in Rubbers, *Macromolecules* **7**, 59 (1974).
- [17] Y. Gu, J. Zhao, and J. A. Johnson, A (Macro)Molecular-Level Understanding of Polymer Network Topology, *Trends in Chemistry* **1**, 318 (2019).
- [18] S. Seiffert, Origin of nanostructural inhomogeneity in polymer-network gels, *Polymer Chemistry* **8**, 4472 (2017).
- [19] J. Bastide and L. Leibler, Large-scale heterogeneities in randomly cross-linked networks, *Macromolecules* **21**, 2647 (1988).
- [20] F. Ikkai and M. Shibayama, Inhomogeneity control in polymer gels, *Journal of Polymer Science Part B: Polymer Physics* **43**, 617 (2005).
- [21] M. A. Bibbo and E. M. Valles, Calculation of average properties of the pendant chains in a network, *Macromolecules* **15**, 1293 (1982).
- [22] K. Dušek, M. Dušková-Smrčková, J. J. Fedderly, G. F. Lee, J. D. Lee, and B. Hartmann, Polyurethane networks with controlled architecture of dangling chains, *Macromolecular Chemistry and Physics* **203**, 1936 (2002).
- [23] J. L. Stanford and R. F. T. Stepto, Rate theory of irreversible linear random polymerisation. Part 1. Basic theory, *Journal of the Chemical Society, Faraday Transactions 1: Physical Chemistry in Condensed Phases* **71**, 1292 (1975).
- [24] J. L. Stanford, R. F. T. Stepto, and D. R. Waywell, Rate theory of irreversible linear random polymerisation. Part 2. Application to intramolecular reaction in AA + BB type polymerisations, *Journal of the Chemical Society, Faraday Transactions 1: Physical Chemistry in Condensed Phases* **71**, 1308 (1975).
- [25] Z. Ahmad and R. F. T. Stepto, Approximate theories of gelation, *Colloid and Polymer Science* **258**, 663 (1980).
- [26] V. Schamboeck, P. D. Iedema, and I. Kryven, Dynamic Networks that Drive the Process of Irreversible Step-Growth Polymerization, *Scientific Reports* **9**, 1 (2019).
- [27] R. Wang, A. Alexander-Katz, J. A. Johnson, and B. D. Olsen, Universal Cyclic Topology in Polymer Networks, *Physical Review Letters* **116**, 188302 (2016).
- [28] T.-S. Lin, R. Wang, J. A. Johnson, and B. D. Olsen, Topological Structure of Networks Formed from Symmetric Four-Arm Precursors, *Macromolecules* **51**, 1224 (2018).
- [29] D. Kroll and S. Croll, Heterogeneity in polymer networks formed by a single copolymerization reaction: II. Post-gelation structure and pendants, *Polymer* **116**, 113 (2017).
- [30] D. Kroll and S. Croll, Influence of crosslinking functionality, temperature and conversion on heterogeneities in polymer networks, *Polymer* **79**, 82 (2015).
- [31] A. Balabanyan, E. Kramarenko, I. Ronova, and A. Khokhlov, Monte Carlo study of structure and kinetics of formation of end-linked polymer networks, *Polymer* **46**, 4248 (2005).
- [32] N. Gilra, C. Cohen, and A. Z. Panagiotopoulos, A Monte Carlo study of the structural properties of end-linked polymer networks, *The Journal of Chemical Physics* **112**, 6910 (2000).
- [33] Y. Leung and B. E. Eichinger, Computer simulation of endlinked elastomers. II. Bulk cured tetrafunctional networks, *The Journal of Chemical Physics* **80**, 3885 (1984).
- [34] Y. Leung and B. E. Eichinger, Computer simulation of endlinked elastomers. I. Trifunctional networks cured in the bulk, *The Journal of Chemical Physics* **80**, 3877 (1984).
- [35] N. Hosono, Y. Masubuchi, H. Furukawa, and T. Watanabe, A molecular dynamics simulation study on polymer networks of end-linked flexible or rigid chains, *The Journal of Chemical Physics* **127**, 164905 (2007).
- [36] T. Chou and M. R. D’Orsogna, Coarsening and accelerated equilibration in mass-conserving heterogeneous nucleation, *Physical Review E* **84**, 011608 (2011).
- [37] M. R. D’Orsogna, G. Lakatos, and T. Chou, Stochastic self-assembly of incommensurate clusters, *The Journal of Chemical Physics* **136**, 084110 (2012).
- [38] R. Yvinec, M. R. D’Orsogna, and T. Chou, First passage times in homogeneous nucleation and self-assembly, *The Journal of Chemical Physics* **137**, 244107 (2012), arXiv:1211.1093.
- [39] M. R. D’Orsogna, B. Zhao, B. Berenji, and T. Chou, Combinatoric analysis of heterogeneous stochastic self-assembly, *The Journal of Chemical Physics* **139**, 121918 (2013).
- [40] J. K. Davis and S. S. Sindi, A mathematical model of the dynamics of prion aggregates with chaperone-mediated fragmentation, *Journal of Mathematical Biology* **72**, 1555 (2016).
- [41] D. R. Miller and C. W. Macosko, A New Derivation of Post Gel Properties of Network Polymers, *Macromolecules* **9**, 206 (1976).
- [42] C. W. Macosko and D. R. Miller, A New Derivation of Average Molecular Weights of Nonlinear Polymers, *Macromolecules* **9**, 199 (1976).
- [43] M. W. Tibbitt, A. M. Kloxin, and K. S. Anseth, Modeling controlled photodegradation in optically thick hydrogels, *Journal of Polymer Science Part A: Polymer Chemistry* **51**, 1899 (2013).
- [44] S. C. P. Norris, T. Chou, and A. M. Kasko, Diffusion of Photoabsorbing Degradation Byproducts in Photodegradable Polymer Networks, *Macromolecular The-*

- ory and Simulations **26**, 1700007 (2017).
- [45] C. N. Bowman and C. J. Kloxin, Covalent Adaptable Networks: Reversible Bond Structures Incorporated in Polymer Networks, *Angewandte Chemie International Edition* **51**, 4272 (2012).
- [46] M. C. Roberts, M. C. Hanson, A. P. Massey, E. A. Karren, and P. F. Kiser, Dynamically Restructuring Hydrogel Networks Formed with Reversible Covalent Crosslinks, *Advanced Materials* **19**, 2503 (2007).
- [47] B. Yang, Y. Zhang, X. Zhang, L. Tao, S. Li, and Y. Wei, Facilely prepared inexpensive and biocompatible self-healing hydrogel: a new injectable cell therapy carrier, *Polymer Chemistry* **3**, 3235 (2012).
- [48] C. B. Rodell, R. J. Wade, B. P. Purcell, N. N. Dusaj, and J. a. Burdick, Selective Proteolytic Degradation of Guest/Host Assembled, Injectable Hyaluronic Acid Hydrogels, *ACS Biomaterials Science & Engineering* **1**, 277 (2015).
- [49] C. Yang, F. W. DelRio, H. Ma, A. R. Killaars, L. P. Basta, K. A. Kyburz, and K. S. Anseth, Spatially patterned matrix elasticity directs stem cell fate, *Proceedings of the National Academy of Sciences* **113**, E4439 (2016).
- [50] C. Li and A. Strachan, Free volume evolution in the process of epoxy curing and its effect on mechanical properties, *Polymer* **97**, 456 (2016).
- [51] D. R. Griffin and A. M. Kasko, Photodegradable Macromers and Hydrogels for Live Cell Encapsulation and Release, *Journal of the American Chemical Society* **134**, 13103 (2012).
- [52] C. Xue, D. Y. Wong, and A. M. Kasko, Complex Dynamic Substrate Control: Dual-Tone Hydrogel Photoreagents Allow Double-Dissociation of Topography and Modulus, *Advanced Materials* **26**, 1577 (2014).
- [53] E. Käpylä, S. M. Delgado, and A. M. Kasko, Shape-Changing Photodegradable Hydrogels for Dynamic 3D Cell Culture, *ACS Applied Materials & Interfaces* **8**, 17885 (2016).
- [54] S. C. P. Norris, S. M. Delgado, and A. M. Kasko, Mechanically robust photodegradable gelatin hydrogels for 3D cell culture and in situ mechanical modification, *Polymer Chemistry* **10**, 3180 (2019).
- [55] D. Y. Wong, D. R. Griffin, J. Reed, and A. M. Kasko, Photodegradable Hydrogels to Generate Positive and Negative Features over Multiple Length Scales, *Macromolecules* **43**, 2824 (2010).
- [56] S. C. P. Norris, P. Tseng, and A. M. Kasko, Direct Gradient Photolithography of Photodegradable Hydrogels with Patterned Stiffness Control with Submicrometer Resolution, *ACS Biomaterials Science & Engineering* **2**, 1309 (2016).